ECS Transactions, 80 (9) 111-118 (2017)
10.1149/08009.0111ecst ©The Electrochemical Society

Electric Field-assisted Pressureless Sintering of Ceramic Protonic Conductors

R. Muccillo[a,b*], V. Esposito[c], D.Z. de Florio[b], and E.N.S. Muccillo[a]

[a] Center of Science and Technology of Materials, Energy and Nuclear Research Institute Travessa R 400, Cidade Universitária, S. Paulo, SP, 05508-170, Brazil
[b] Center of Engineering, Modeling and Applied Social Sciences, Federal University of ABC, Av. dos Estados 5001, Santo André, SP, 09210-580, Brazil
[c] Department of Energy Conversion and Storage, Technical University of Denmark Risø DTU Campus, Frederiksborgvej 399, 4000 Roskilde, Denmark

Gadolinium, yttrium and samarium-doped barium cerate pressed pellets were submitted to flash sintering experiments isothermally in the temperature range 800-1300ºC under 200 V cm^{-1} electric field. The pellets were positioned inside a dilatometer furnace with Pt-Ir electrodes connected either to a power supply or to an impedance analyzer to evaluate the bulk and the grain boundary contributions to the electrical resistivity. Near full density was achieved in the sintered samples. The combined results of dilatometry and impedance measurements in conventionally and flash sintered specimens show substantial improvement of the electrical conductivity. Joule heating is assumed to be the primary effect for sintering. Improved grain-to-grain contact and the removal of depleted chemical species due to Joule heating at the space charge region are proposed, respectively, as the reasons for the decrease of the grain boundary component in the impedance diagrams and the improvement of the bulk electrical conductivity.

Introduction

Even though doped barium cerate and barium zirconate have been proposed to be used as solid electrolytes in solid oxide fuel cells operating at temperatures lower than the necessary in SOFCs with yttria stabilized zirconia, two disadvantages are still to be solved (1-4): low sinterability at temperatures available in commercial furnaces and blocking of protons at grain boundaries. The former has been proposed to be overcome either using sintering aids (5-8), powders produced by chemical routes (9-14) or sinteractive nanosize powder particles; the latter by using thin films prepared by different techniques (15,16). Recently an electric field pressureless sintering of ceramics has been used to sinter solid electrolytes at temperatures lower than conventional producing consolidated bodies without considerable grain growth (17-24). In short, sintering to near full density is achieved by applying moderate electric fields (~ 100 V cm^{-1}) with limiting currents (mA to few A range) to green ceramic pellets upon heating (dynamic process) or isothermally at chosen temperatures below the conventional temperature for sintering (25). That sintering technique, hereafter flash sintering (FS) when the shrinkage-consolidation event lasts few seconds, which is the time the electric current pulse traverses the specimen submitted to an electric field, is applied here to proton conductors at temperatures well below the required for high densification of the same proton conductors.

Experimental

$BaCe_{0.9}Sm_{0.1}O_{3-\delta}$, $BaCe_{0.9}Gd_{0.1}O_{3-\delta}$ and $BaCe_{0.9}Y_{0.1}O_{3-\delta}$ powders were synthesized by the liquid mix technique (26,27) with calcination at 450°C/1 h for elimination of organic residuals. The experimental setup for sintering green pellets under an electric field consisted on a vertical dilatometer (model 1161, Anter, USA) with the sample holder electrically connected with Pt-Ir leads to a custom made power supply (70 Vac, 500-1100 Hz, 0.5A-5A current limit control). Further details may be found in previous papers (25,28-31). The experimental procedure for isothermal flash sintering consisted on i) heating the specimen in the dilatometer furnace, ii) applying an electric field at chosen temperature (Figure 1). The electric field is applied up to the occurrence of an electric current pulse, and kept on up to no shrinkage is detected in the dilatometer gauge, monitored accurately (±1 μm); the temperature is monitored with a Pt-Pt10%Rh thermocouple with its tip positioned close to the specimen. Electric voltage and electric current data are monitored with two Fluke 8050A multimeters and collected in a data logger. A typical example of their profiles during flash sintering is shown in Figure 1.

Impedance spectroscopy measurements were carried out with a Hewlett Packard 4192A impedance analyzer. Three cylindrical samples, with their parallel surfaces covered with silver paste, were inserted in a sample chamber, positioned inside a programmable furnace. [-Z''(ω) x Z'(ω)] impedance data were collected at 390°C in the 5 Hz-13 MHz frequency range, 200 mV applied bias, with a special software (32).

X-ray diffraction analyses were performed in a Bruker-AXS D8 Advance diffractometer with a Bragg-Brentano θ-2θ configuration, Cuk_{α} radiation, 10-90 2θ range, 0.05° step size, 5 s per step.

Thermogravimetric analyses of the ceramic powders were carried out in a Netzsch STA 409E flowing synthetic air, 5 L min^{-1}, from room temperature to 1500°C.

Scanning electron microscopy images were observed in polished and 1400°C/15 min thermally etched flat surfaces of the sintered pellets in a FEG-SEM Inspect F50 microscope.

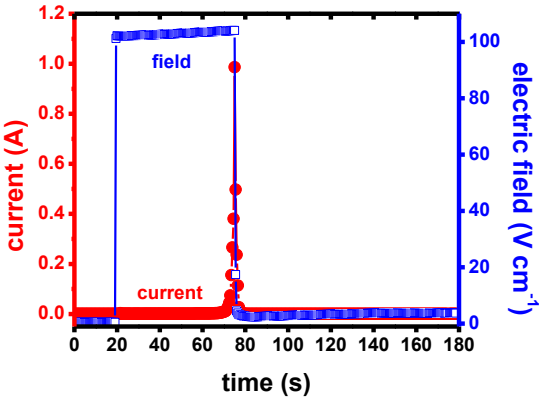

Figure 1. Applied electric field and current pulse during electric field-assisted pressureless (flash) sintering.

Results and Discussion

Figure 1 shows X-ray diffraction patterns of 10 mol% Gd-, Sm- and Y-doped $BaCeO_3$. The patterns are similar and correspond to the $BaCeO_3$ compound (JCPDS 71-2394).

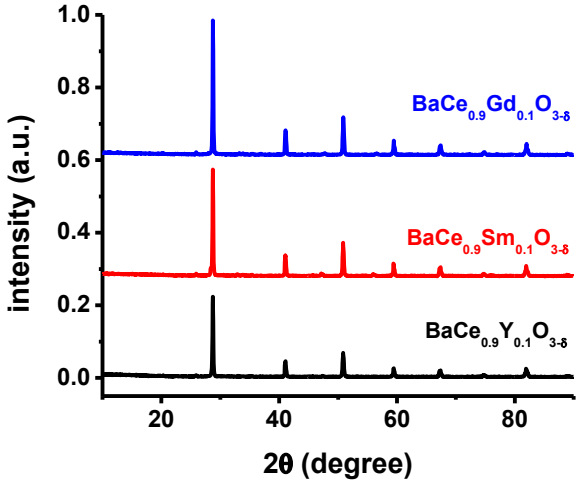

Figure 2. X-ray diffraction patterns of $BaCe_{0.9}Gd_{0.1}O_{3-\delta}$ (top), $BaCe_{0.9}Sm_{0.1}O_{3-\delta}$ (middle) and $BaCe_{0.9}Y_{0.1}O_{3-\delta}$ (bottom) powders.

The results of thermogravimetric analysis of the powders are shown in Figure 3. After a 5% mass decrease from room temperature to approximately 750°C another 5% decrease happens from that temperature to 1125°C. The former is probably due to release of physisorbed water and the latter for release of carbon dioxide known to be attached to barium cerate from the atmosphere during handling.

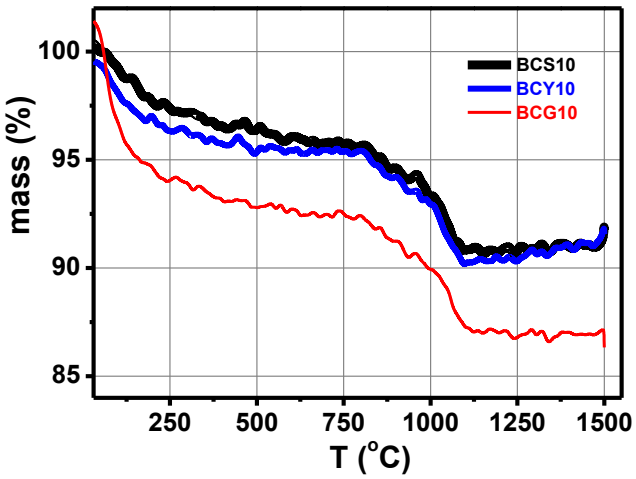

Figure 3. Thermogravimetric curves of $BaCe_{0.9}Sm_{0.1}O_{3-\delta}$, $BaCe_{0.9}Y_{0.1}O_{3-\delta}$ and $BaCe_{0.9}Gd_{0.1}O_{3-\delta}$ powders from room temperature to 1500°C in air; heating rate 10 deg/min.

The powders were pressed to pellets for flash sintering experiments inside the dilatometer. Apparent geometrical green densities were in the 40-45% of the theoretical density. Upon heating, all dilatometric curves show a first and a second shrinkage, meaning that mass is lost, in good agreement with the thermogravimetric analyses (Figure 3). Reaching the temperatures for application of the electric field, similar

specimens of the three (Gd-, Sm- and Y-doped barium cerates) were submitted to flash sintering at two pre-set temperatures, 1200ºC and 1300ºC. The dilatometric results measured upon application of approximately 200 V cm^{-1} AC electric fields (f = 1.1 kHz) during 5 min at these two temperatures are shown in Figure 3a ($BaCe_{0.9}Gd_{0.1}O_{3-\delta}$), 3b ($BaCe_{0.9}Sm_{0.1}O_{3-\delta}$) and 3c ($BaCe_{0.9}Y_{0.1}O_{3-\delta}$). These figures show also the dilatometric curves of similar specimens heated up to 1500ºC. The behavior of the 3 figures is apparently the same: the conventional sintering to 1500ºC follows at least two stages, the first from room temperature to approximately 1200ºC, and the second from that temperature to the maximum shrinkage. Let's now to analyze each figure:

- the gadolinium-doped sample, Figure 3a, achieves 18.4% shrinkage level after flash sintering at 1200ºC, 22.5% conventionally sintered at 1500ºC and an impressive 45.6% after flash sintering at 1300ºC, an addition of 27.2% comparing to flash sintering at 100 degrees lower temperature. The main conclusion here is that the application of an electric field at 1300ºC produces a two-fold decrease of the specimen thickness than sintering at 1500ºC without applying an electric field.
- the samarium-doped samples, Figure 3b, reach 20.4% and impressive 40.6% thickness shrinkages after flash sintering at 1200ºC and 1300ºC, respectively. The specimen conventionally sintered at 1500ºC shows a thickness shrinkage of 33.9%.
- the yttrium-doped samples, Figure. 3c, flash sintered at 1200ºC and 1300ºC shrank 27.4% and 33.5%, both values higher than sintering by heating up to 1500ºC (15.8%).

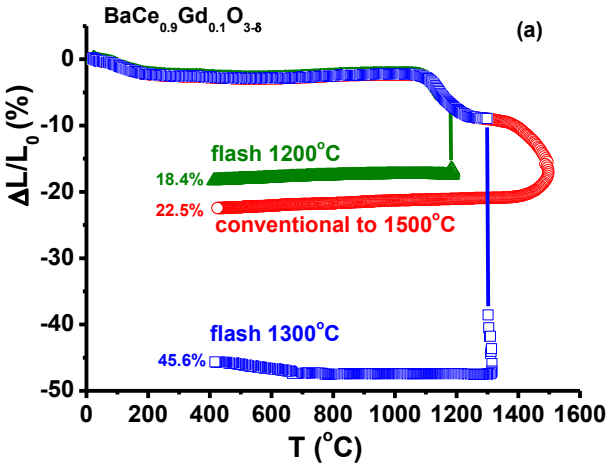

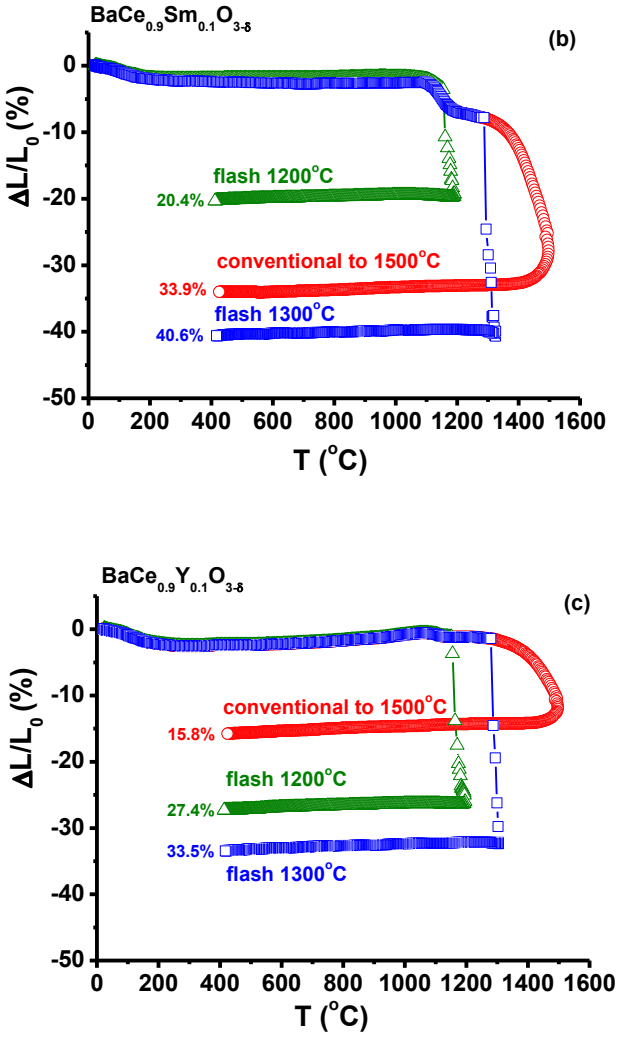

Figure 3: Dilatometric curves (thickness shrinkage) of **(a)** $BaCe_{0.9}Gd_{0.1}O_{3-\delta}$, **(b)** $BaCe_{0.9}Sm_{0.1}O_{3-\delta}$ and **(c)** $BaCe_{0.9}Y_{0.1}O_{3-\delta}$ pellets sintered by applying 200 V cm^{-1} at 1100 Hz during 5 min, limiting the current to 5A. Temperature of the electric field application: 1200ºC (green △) and 1300ºC (blue □). Conventional sintering (no applied electric field) (red o).

All specimens flash sintered at 1200ºC had their parallel surfaces painted with silver paste, cured at 400ºC for collection of impedance spectroscopy data at 390ºC. The results are shown in Figure 4. The total electrical resistivity of the specimens flash sintered at 1200ºC is several times lower than in the specimens sintered at 1500ºC without the application of the electric field. Moreover, the impedance diagrams of the flash sintered samples are apparently composed of mainly two semicircles in the measured frequency range, due to intergranular (lower frequency region) and to intragranular (bulk, higher frequency) components of the electrical resistivity (Figure 4d).

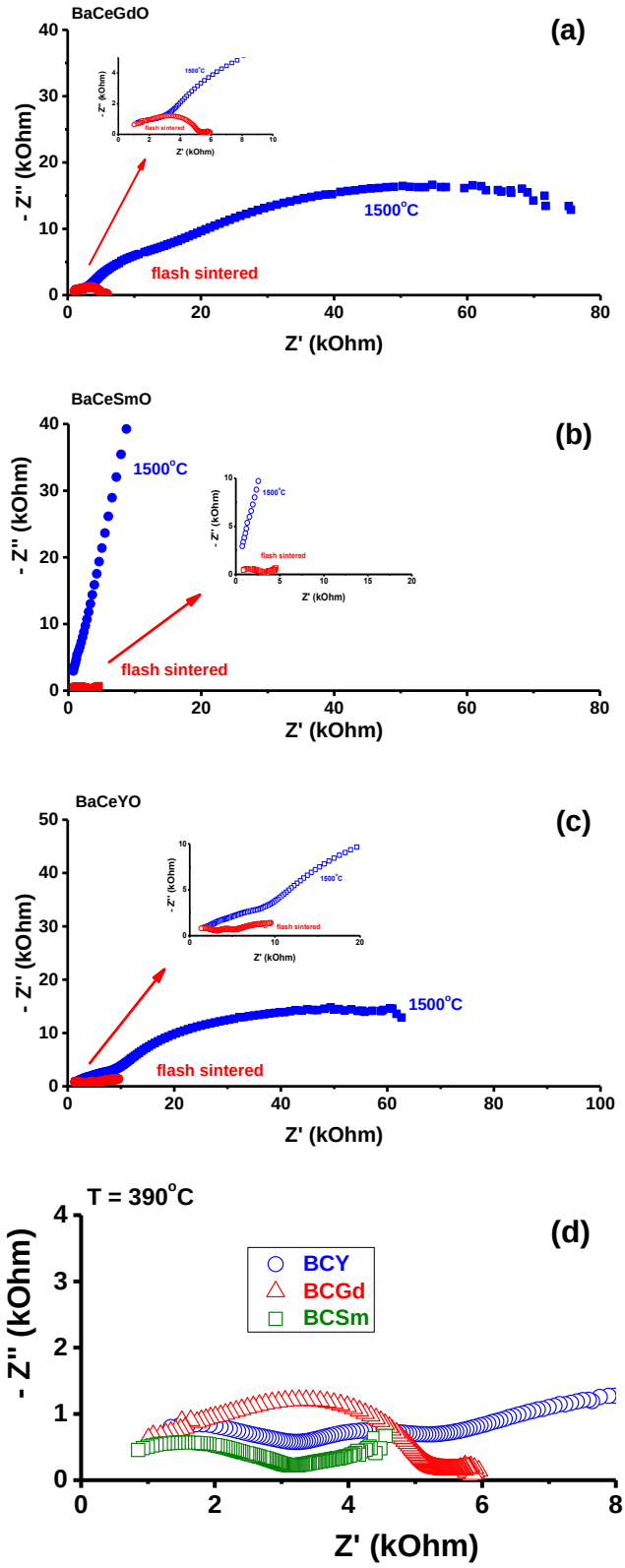

Figure 4: Impedance diagrams in the 10 Hz-10 MHz range of **(a)** $BaCe_{0.9}Gd_{0.1}O_{3-\delta}$; **(b)** $BaCe_{0.9}Sm_{0.1}O_{3-\delta}$; **(c)** $BaCe_{0.9}Y_{0.1}O_{3-\delta}$ pellets sintered at 1500°C and flash sintered at 1180°C; and **(d)** all samples flash sintered at 1080°C. Temperature of measurement: 390°C. Insets: zoom at the high frequency region.

The main difference in resistivity is apparently in the grain boundary resistivity. It is well known that one of the challenges for obtaining barium zirconate-based proton conductors with electrical resistivity suitable for replacing yttria-stabilized zirconia remains in decreasing the blocking of protons at the interfaces. One could speculate that the reason for obtaining, by flash sintering, dense and with low grain boundary resistivity yttrium-doped barium cerate is the work developed by the electric current pulse at the interfaces of the specimen. The primary reason is evidently the huge increase in the local temperature due to Joule heating, which could improve the grain-to-grain contact and possibly dissolving chemical species, depleted at the space charge region, back to the grains (25). This would increase the oxide ion vacancy concentration, decreasing the electrical resistivity, as indicated by the impedance diagrams.

Conclusions

Gadolinium, samarium and yttrium-doped barium cerate powders, synthesized by the liquid mix technique and pressed to pellets, were successfully sintered to near full density by electric field-assisted pressureless sintering with 200 V cm^{-1} at 1.1 kHz during 5 min at 1200^{o}C and 1300^{o}C. The grain boundary resistivity of the sintered specimens shows a huge decrease in comparison with specimens conventionally sintered at 1500^{o}C. Joule heating is proposed as the primary mechanism responsible for modifying the space charge region in such way that diffusion to the bulk of chemical species depleted at the grain boundaries decreases the bulk resistivity, and the blocking of protons is inhibited at the interfaces.

Acknowledgments

To CNEN, CNPq (Procs. 470952/2013-0 and 303483/2013-0) and FAPESP (CEPID-CDMF, Proc. 2013/07296-2) for financial support.

References

1. K.D. Kreuer, *Annu. Rev. Mater. Res.*, **33**, 333 (2003).
2. H.G. Bohn and T. Schober, *J. Am. Ceram. Soc.*, **83**, 768 (2000).
3. E.C.C. de Souza and R. Muccillo, *Mater. Res.*, **13**, 385 (2010).
4. L. Bi, Z.T.Tao, R.R. Peng, and W. Liu, *J. Inorg. Mater.*, **25**, 1 (2010).
5. P. Babilo and S.M. Haile, *J. Am. Ceram. Soc.*, **88**, 2362 (2005).
6. S.B.C. Duval, P. Holtappels, U. Stimming, and T. Graule, *Solid State Ionics*, **179**, 21 (2008).
7. C. Duan, J. Tong, M. Shang, S. Nikodemski, M. Sanders, S. Ricote, A. Almansoori, and R. O'Hayre, *Science*, **349**, 6254, 1321 (2015).
8. S. Ricote and N. Bonanos, *Solid State Ionics*, **181**, 694 (2010).
9. A. Magrez, *Solid State Ionics*, **175**, 585 (2004).
10. Y. Yamazaki, P. Babilo, and S.M. Haile, *Chem. Mater.*, **20**, 6352 (2008).
11. B. Bendjeriou-Sedjerari, J. Loricourt, D. Goeuriot, and P. Goeuriot, *J. Alloys Compd.*, **509**, 6175 (2011).
12. P.I. Dahl, H.L. Lein, Y. Yu, J. Tolchard, T. Grande, M.-A. Einarsrud, C. Kjølseth, T. Norby, and R. Haugsrud, *Solid State Ionics*, **182**, 32 (2011).
13. M.D. Gonçalves and R. Muccillo, *Ceram. Int.*, **40**, 911 (2014).
14. F. Bozza, Y. Arroyo, and T. Graule, *Fuel Cells*, **15**, 588 (2015).

15. V. Agarwal and M.L. Liu, *J. Mater. Sci.*, **32**, 619 (1997).
16. D. Pergolesi, E. Fabbri, A. D'Epifanio, E. Di Bartolomeo, A. Tebano, S. Sanna, S. Licoccia, G. Balestrino, and E. Traversa, *Nature Mater.*, **9**, 846 (2010).
17. S. Ghosh, A.H. Chokshi, P. Lee, and R. Raj, *J. Am. Ceram. Soc.*, **92**, 1856 (2009).
18. D. Yang, R. Raj, and H. Conrad, *J. Am. Ceram. Soc.*, **93**, 2935 (2010).
19. M. Cologna, B. Rashkova, and R. Raj, *J. Am. Ceram. Soc.*, **93**, 3556 (2010).
20. D. Yang and H. Conrad, *Scripta Mater.*, **63**, 328 (2010).
21. R. Muccillo, M. Kleitz, and E.N.S. Muccillo, *J. Eur. Ceram. Soc.*, **31**, 517 (2011).
22. S. Grasso, Y. Sakka, N. Rendtorff, C. Hu, G. Maizza, H. Borodianska, and O. Vasylkiv, *J. Ceram. Soc. Japan*, **119**, 144 (2011).
23. M. Cologna and R. Raj, *J. Am. Ceram. Soc.*, **94**, 391 (2011).
24. M. Cologna, A.L.G. Prette, and R. Raj, *J. Am. Ceram. Soc.*, **94**, 316 (2011).
25. R. Muccillo and E.N.S. Muccillo, *J. Electroceram.*, **28**, 34 (2017).
26. V. Esposito, C. D`Ottavi, S. Ferrari, S. Licoccia, and E. Traversa, in *Proc. 8th Int. Symp. Solid Oxide Fuel Cells*, S.C. Singhal and M. Dokiya, Editors, p. 643, The Electrochem. Soc., New York (2002).
27. V. Esposito, D.Z. de Florio, F.C. Fonseca, E.N.S. Muccillo, R. Muccillo, and E. Traversa, *J. Eur. Ceram. Soc.*, **25**, 2637 (2005).
28. R. Muccillo and E.N.S. Muccillo, *J. Eur. Ceram. Soc.*, **33**, 515 (2013).
29. R. Muccillo and E.N.S. Muccillo, *J. Eur. Ceram., Soc.*, **34**, 3871 (2014).
30. R. Muccillo and E.N.S. Muccillo, *J. Eur. Ceram. Soc.*, **34**, 915 (2014).
31. E.N.S. Muccillo and R. Muccillo, *J. Eur. Ceram. Soc.*, **34**, 3699 (2014).
32. M. Kleitz and J. H. Kennedy, in *Fast Ion Transport in Solids/1979*, P. Vashishta, J. N. Mundy and G. K. Shenoy, Editors, p. 185, Elsevier North Holland, The Netherlands (1979).